doi:10.1006/jmbi.2001.5402 available online at http://www.idealibrary.com on IDEAL® *J. Mol. Biol.* (2002) **316**, 1101–1110

JMB

Structure, Dynamics and Binding Characteristics of the Second PDZ Domain of PTP-BL

Tine Walma[1], Christian A. E. M. Spronk[1], Marco Tessari[1], Jan Aelen[1] Jan Schepens[2], Wiljan Hendriks[2] and Geerten W. Vuister[1]*

[1]*NSR-RIM Center, Department of Biophysical Chemistry University of Nijmegen Toernooiveld 1, 6525 ED Nijmegen, The Netherlands*

[2]*Institute of Cellular Signaling Department of Cell Biology University of Nijmegen, Geert Grooteplein 28, 6525 GA Nijmegen, The Netherlands*

**Corresponding author*

The PDZ domains of the protein tyrosine phosphatase PTP-BL mediate interactions by binding to specific amino acid sequences in target proteins. The solution structure of the second PDZ domain of PTP-BL, PDZ2, displays a compact fold with six β strands and two α-helices. A unique feature of this domain compared to the canonical PDZ fold is an extended flexible loop at the base of the binding pocket, termed L1, that folds back onto the protein backbone, a feature that is shared by both the murine and human orthologues. The structure of PDZ2 differs significantly from the orthologous human structure. A comparison of structural quality indicators clearly demonstrates that the PDZ2 ensemble is statistically more reasonable than that of the human orthologue. The analysis of ^{15}N relaxation data for PDZ2 shows a normal pattern, with more rigid secondary structures and more flexible loop structures. Close to the binding pocket, Leu85 and Thr88 display greater mobility when compared to surrounding residues. Peptide binding studies demonstrated a lack of interaction between murine PDZ2 and the C terminus of the murine Fas/CD95 receptor, suggesting that the Fas/CD95 receptor is not an *in vivo* target for PDZ2. In addition, PDZ2 specifically binds the C termini of both human Fas/CD95 receptor and the RIL protein, despite RIL containing a non-canonical PDZ-interacting sequence of E-x-V. A model of PDZ2 with the RIL peptide reveals that the PDZ2 binding pocket is able to accommodate the bulkier side-chain of glutamic acid while maintaining crucial protein to peptide hydrogen bond interactions.

Keywords: PDZ; PTP-BL; LIM; Fas/CD95; solution structure and dynamics

Introduction

PTP-BL is a 270 kDa mouse protein tyrosine phosphatase that contains an N-terminal domain that lacks homology to other protein types, a FERM domain, five PDZ domains (denoted PDZ1 through PDZ5) and a C-terminal catalytic phosphatase domain.[1] Localization studies have placed PTP-BL in the submembranous region of epithelial cells;[2] however, the identities of its *in vivo* substrates are presently unknown. Several candidate proteins have been identified on the basis of their association with the PDZ domains of PTP-BL (Figure 1). In particular, PDZ2 and PDZ4 interact with two LIM domain-containing proteins, RIL and TRIP-6,[3] which are found at actin-rich structures in the cell. In addition, PDZ1 can interact with BP75,[4] PDZ2 with the tumor suppressor protein APC[5] and PDZ3 with the Rho effector kinase PRK2.[6]

For the human orthologue of PTP-BL, PTP-Bas (also known as PTPL1, FAP-1, PTP1E, or PTPN13),

Abbreviations used: PDZ, PSD-95/Dlg/ZO-1; PTP-BL, protein tyrosine phosphatase BAS-like; PTP-Bas, protein tyrosine phosphatase-basophile; TRIP-6, thyroid receptor interacting protein-6; RIL, reversion-induced LIM; LIM, Lin-11/Isl-1/Mec-3; DglA, discs large protein A; CASK, calcium/calmodulin-dependent serine kinase; nNOS, neuronal nitric oxide synthase; APC, adenomatous polyposis coli; NOE, nuclear Overhauser enhancement; NOESY, NOE spectroscopy; TOCSY, total correlated spectroscopy; TROSY, transverse relaxation optimized spectroscopy; HSQC, heteronuclear single quantum coherence.

E-mail address of the corresponding author: vuister@nmr.kun.nl

0022-2836/02/051101–10 $35.00/0

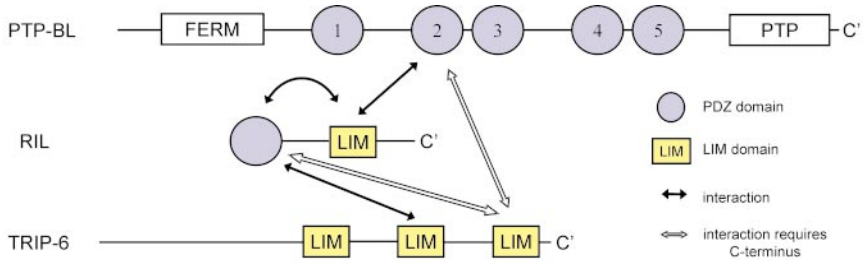

Figure 1. Schematic outline of some reported intracellular interactions involving PTP-BL. All Figures were prepared using MOLMOL.[39]

a wide variety of PDZ-interaction partners have also been identified. Considerable interest in the literature has been shown in the reported interactions of PDZ2 and PDZ4 with the Fas/CD95 receptor,[7,8] an interaction that does not seem to be conserved in mouse.[9] In addition, human PDZ1 has been reported to interact with IκBα,[10] PDZ2 with p75(NTR),[11] PDZ4 with the Rho-GAP PARG1[12] and with B class ephrins.[13] Although the physiological relevance for the observed interactions is still under study, current data indicate that PTP-BL/PTP-Bas plays a role in the organization of the cell cortical actin cytoskeleton, and perhaps in Fas-mediated apoptosis of human cells. The mechanism by which the PDZ domains of PTP-BL and PTP-Bas mediate such interactions requires further elucidation.

Many PDZ domain-containing proteins interact with transmembrane proteins such as receptors and channels, or membrane-associated proteins. Three types of interaction involving PDZ motifs have previously been described in detail. The first two types of interactions, class 1 and class 2, involve binding of terminal protein sequences while the third type binds internal sequences. Class 1 interactions involve protein C termini with a (S/T)-x-(V/I/L) sequence motif.[14] Examples of this interaction include DglA,[14] PSD-95[15] and most recently NHERF.[16] Class 2 interactions involve C termini containing a -(F/Y)-x-(F/V/A) sequence motif,[14] behavior exhibited by CASK[17] and INAD.[18] The third type of interaction involves PDZ binding to an internal -(S/T)-x-V- sequence motif, as exhibited by the PDZ-PDZ dimerization interaction between syntrophin and nNOS.[19] Exceptions to these binding rules are known to exist, for example the nNOS PDZ domain binds -G(D/E)-x-V sequences[20] and syntenin binds IL-5Rα *via* a -S-x-F motif[21], both modifications of the class 1 requirements.

PDZ domains adopt an α/β fold consisting of a partly open barrel formed by six β-strands, termed β1 to β6, and capped by two α-helices, termed α1 and α2. Ligand proteins bind to PDZ domains *via* a binding pocket located between β2 and α2, creating an extension to the existing β-sheet. Crucial PDZ-ligand interactions include backbone hydrogen bonds between β2 and the ligand, interactions between the ''carboxylate binding loop'' (located between β1 and β2) and the inserted -COOH terminus, and finally side-chain charge and steric requirements for the 0 (or C-terminal) and −2 residues of the ligand protein. The structural basis for other reported PDZ interactions are unknown, most notably interactions of PDZ domains with ankyrin repeats[10] and LIM domains.[2] For example, using a two-hybrid interaction trap, Cuppen *et al.*[2] showed that the interaction between PDZ2 and RIL-LIM required the complete LIM domain, exclusive of the final four or 21 RIL C-terminal residues, and that binding of the PDZ2 to the C terminus alone was not detectable. These observations suggest a mechanism distinct from canonical PDZ interactions. Two possible explanations for this PDZ-LIM interaction can be envisioned. It could involve binding an internal sequence, analogous to the syntrophin-nNOS interaction, or it could involve a yet undiscovered binding surface on the PDZ and/or LIM domain. The latter hypothesis is supported by the discovery that PDZ scaffolding interactions are crucial in forming a ternary complex between PSD-95, nNOS and NMDA, and that the two binding faces of the PDZ domain of nNOS are capable of functioning simultaneously.[22]

It has become clear that the mechanisms of PDZ-ligand binding are more diverse than previously thought. Therefore, we present here the structure and dynamics of the second PDZ domain of PTP-BL and its interactions with Fas receptor and RIL protein C termini. Our results provide additional data on the binding preferences of PDZ2 and putative *in vivo* binding partners of PTP-BL.

Results

Using high-resolution heteronuclear NMR spectroscopy, as outlined in Materials and Methods, we calculated an ensemble of 35 high-resolution NMR structures of the PDZ2 domain of PTP-BL, comprising residues 1351 to 1444 (corresponding to our 9 through 102 numbering convention of our construct). A stereo view of the best superimposition of this ensemble is shown in Figure 2(a). The structural ensemble was analyzed statistically using the programs PROCHECK-NMR[23] and WHAT-IF;[24] statistics for the ensemble are reported

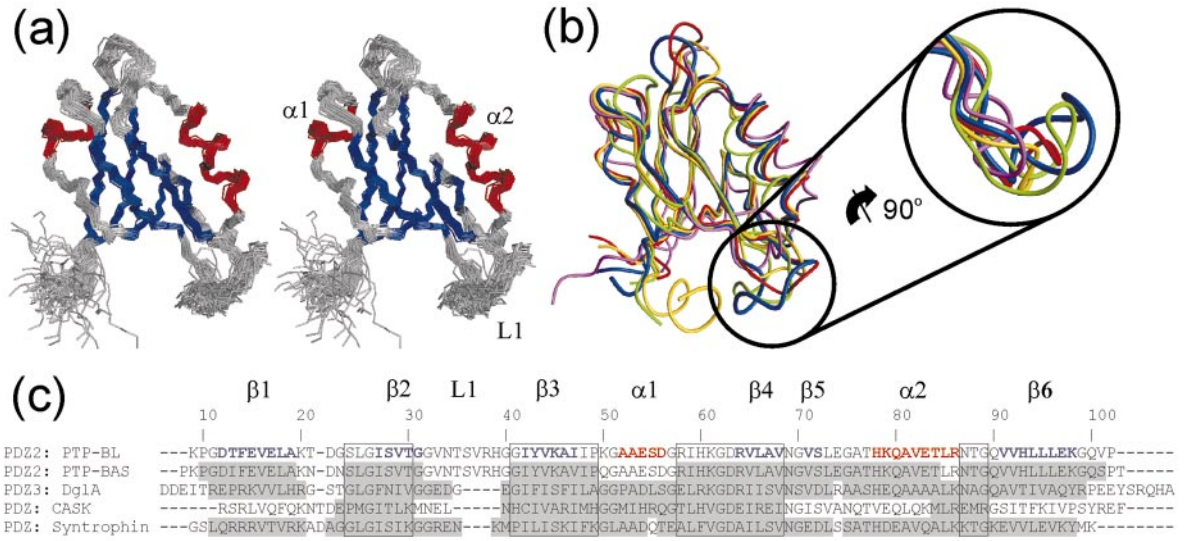

Figure 2. (a) Structural ensemble of 35 PDZ2 structures (stereo diagram). (b) Structural superposition of PDZ2 (blue) with PDZ domains from PTP-Bas (green), DlgA (yellow), CASK (magenta) and syntrophin (red). Detail of the flexible loop region (circle): PDZ2 and its human orthologue possess an extended loop L1. (c) Sequence alignment corresponding to the structural superposition in (b). Secondary structures of PDZ2 are indicated by blue (β-strand) and red (α-helix) color-coding. Regions that are structurally conserved with respect to PDZ2 (as calculated by WHAT-IF[24]) are shaded gray. Boxes surround regions that are structurally conserved across all three class representatives and contain residues that were used in RMSD comparisons.

in the first column of Table 1. The second column of Table 1 contains corresponding statistics for the human orthologue of PDZ2 (*vide infra*). All accepted PDZ2 structures contain no distance violations >0.5 Å and no dihedral angle violations >5° from experimental data. The ensemble was calculated using approximately 16 distance restraints per residue (1489 distance restraints), 59 hydrogen bonding restraints and 154 dihedral angle restraints. The pairwise RMSD of ordered backbone heavy atoms is 0.52(±0.09) Å, indicating a well-defined ensemble. The pairwise RMSD of the global backbone heavy atoms gives a larger value of 1.39(±0.36) Å. The Ramachandran plot displays 85% of the residues in most favored regions and 13% in additionally allowed regions. The RMS deviation from idealized covalent geometry *Z*-score values are close to unity, indicating that the ensemble exhibits good covalent geometry; these parameters are often weak points of NMR structures.

The ensemble displays a compact fold with six β-strands, β1 through β6, and two α-helices, α1 and α2 (Figure 2(c)). In addition the structure contains five β-turns and one flexible loop (L1) located between β2 and β3. Based on relaxation data, the most flexible regions are the first β-turn, in the loop L1 and the unstructured C terminus (*vide infra*). The L1 loop of PDZ2 (and its human orthologue) is distinct from other known PDZ domains, and consists an insert of three to five residues in comparison to other PDZ domains. Located near the binding pocket, this loop curves back onto the backbone, its conformation defined by distinct NOE contacts between Val37 and Tyr43. The loop is also flanked by two sets of glycine residues (Gly31/32 and Gly40/41) that appear to act as hinges; the loop residues themselves superimpose well (not shown). The N-terminal section of the loop, located directly under the binding pocket, is more structurally defined than the C-terminal half, mainly because of contacts to α2. This loop is subject to alternative splicing that has been shown to affect binding to the APC C terminus.[5]

Structural superposition of PDZ domains

To analyze the structure further, we superposed PDZ2 with four other PDZ structures, the human orthologue of PDZ2 from PTP-Bas (PDB entry 3PDZ), and three representative X-ray structures from each of the known interaction classes: DlgA, CASK and syntrophin (PDB entries 1PDR, 1KWA and 1QAV, respectively). PDZ2 shares the highest sequence identity with PTP-Bas (94% identity). The class 1 type is represented by the X-ray structure of the third PDZ domain of human DlgA. This domain shares a 34% sequence identity with PDZ2. The X-ray structure of the PDZ domain of CASK represents the class 2 domain, sharing 28% identity. The X-ray structure of the PDZ domain of mouse syntrophin, with 39% identity; this domain has been shown to bind nNOS *via* an internal β-hairpin loop, the third type of interaction.

The structures were superposed using the program WHAT-IF;[24] the results are shown in Figure 2(b). The structures were compared using

Table 1. Reported structural statistics for PDZ2 of PTP-BL and its human orthologue

Structural statistics	PDZ2	Human orthologue[a]
A. *Restraint information*[b]		
Distance restraints (Intra-residual/sequential/medium/long)	1489(515/356/185/433)	1261(348/321/135/457)
Hydrogen bonding restraints	59	45
Dihedral angle restraints (phi/psi/chi1/chi2)	154 (79/66/5/4)	81(n/a)
B. *Average RMS deviation from experimental restraints*[b]		
Distance restraints (Å)	0.029 ± 0.00042	0.017 ± 0.01
Dihedral angle restraints (deg.)	0.697 ± 0.1692	n/a
C. *Pairwise Cartesian RMS deviation (Å)*[b]		
Global backbone heavy atoms	1.39 ± 0.36	$0.41 \pm 0\ 09$
Global all heavy atoms	2.39 ± 0.38	1.08 ± 0.10
Ordered[c] backbone heavy atoms	0.52 ± 0.09	n/a
Ordered all heavy atoms	2.19 ± 0.38	n/a
D. *Ramachandran quality parameters (%)*[d]		
Residues in favored regions	85.5	64.6
Residues in allowed regions	13.4	32.7
Residues in additionally allowed regions	0.6	2.1
Residues in disallowed regions	0.5	0.6
E. *Errors found in structural checks*[d]		
Abnormally short interatomic distances	1	1787
Unusual torsion angles	6	259
Unusual backbone torsion angles (ψ/ϕ)	11	293
Unusual backbone oxygen positions	1	139
Unsatisfied H-bond donors (buried)	12	377
Unsatisfied H-bond acceptors (buried)	0	30
F. *Average RMS deviation from current reliable structures (RMS Z-scores, null deviation=1)*[d]		
Bond lengths	1.066	0.256
Bond angles	1.214	0.514
Omega angle restraints	1.493	0.160
Side-chain planarity	1.081	0.057
Improper dihedral distribution	0.870	0.283
Inside/outside distribution	1.001	0.957
G. *Average deviation from current reliable structures (Z-scores, null deviation=0)*[d]		
1st generation packing quality	−2.456	n/a
2nd generation packing quality	−1.157	−2.663
Ramachandran plot appearance	−1.311	−5.108
Chi-1/chi-2 rotamer normality	−1.712	−4.820
Backbone conformation	−1.962	−4.348

[a] PDB accession codes for PDZ2 and its human orthologue are 1GM1 and 3PDZ, respectively.
[b] Data listed for the human orthologue are as reported by Kozlov *et al.*[31]
[c] Residues involved in secondary structure: 12-19, 27-32, 41-47, 52-56, 64-68, 71-72, 78-86 and 91-98.
[d] Values based on WHAT-CHECK[25] output. WHAT-CHECK reports are available for every structure deposited in the RCSB Protein Data Bank.

backbone displacement values. These were calculated using structurally conserved regions (Figure 2(c)) in order to prevent the gross misalignment in L1 from biasing the result. These calculations yielded heavy-atom backbone displacement values of 1.53 Å for PTP-Bas, 0.94 Å for DglA, 0.93 Å for CASK and 1.33 Å for syntrophin. Despite very high sequence homology, the RMSD analysis shows that the human orthologue is the most displaced from PDZ2. This result was surprising as the sequence differences between the two domains occur mainly in loop regions. We also observed that the most significant structural discrepancies between PDZ2 and PTP-Bas occur between their respective β4 strands, α2 helices and L1 loops, and that these discrepancies are caused by different backbone dihedral angles in their loop and turn regions (Lys20-Gly26, Gly31 to Gly41, Pro49-Lys50 and Thr88-Gly89).

To probe the reasons for these differences, we completed an exhaustive comparison of the two structural ensembles using statistics reported by WHAT-CHECK[25] and the published data for the human PDZ2 ensemble. The highlights of this comparison are listed in Table 1. WHAT-CHECK reports are routinely performed for every structure submitted to the RCSB Protein Data Bank and are used as a diagnostic tool in the validation of protein structures. As Table 1 shows, the Ramachandran plot quality for PDZ2 is much higher than that of the human orthologue (86 % *versus* 65 % of residues in most favored regions) and PDZ2 also contains significantly fewer violations of standard protein geometry than the human orthologue does.

For example, the entire ensemble for PDZ2 contains only one interatomic clash whereas 1787 clashes are reported for the human orthologue ensemble. Comparing RMS *Z*-scores shows that, without exception, those reported for PDZ2 are closer to the expected value of 1.0, than those reported for the human orthologue in PTP-Bas. Similarly, comparing *Z*-scores for the two ensembles shows that the scores for PDZ2 are consistently closer to the expected value of zero. Both of these *Z*-score comparisons demonstrate that PDZ2 conforms much better to ideal geometry expected from a high quality subset of X-ray structures culled from the PDB than does the human orthologue. In all, the PDZ2 ensemble should be considered a more reliable representation of this domain than that published for the human orthologue.

We also compared PDZ2 with three X-ray structures representing the three interaction classes. This comparison revealed that the PDZ fold is well conserved despite different interaction mechanisms and considerable lack of sequence similarity. It also shows that the largest structural disparity occurs in the L1 loop region.

Interactions with protein C termini

The interactions of the PDZ2 domain with the C-termini of human Fas receptor, mouse Fas receptor and RIL protein were characterized *via* the titration of appropriate 12-mer peptides to ^{15}N-labelled PDZ2, while monitoring peak differences in ^{15}N HSQC spectra. The human Fas receptor ends with the class 1 PDZ binding sequence, -S-L-V[14] and acted as a positive binding control.[7–9] The mouse Fas receptor peptide contains the terminal sequence -C-L-E, and was not expected to bind.[9] RIL contains the sequence -E-L-V, a modified class 1 sequence, and was included with the aim of clarifying the contribution of the RIL C terminus to the reported PDZ2-RIL interaction.[2] The titration results are shown in Figure 3.

The PDZ2-human Fas receptor peptide complex yielded spectra indicating intermediate exchange. The dissociation constant was calculated to be in the 0.2-0.5 mM range; however, this value should be regarded as an upper limit because the peptide displayed limited solubility at higher concentrations. The mouse Fas receptor peptide interacted weakly and non-specifically with PDZ2, none of the affected residues being associated with the binding pocket. For affected residues, a dissociation constant of ~1.5 mM was determined, indicating that even with non-specific binding, PDZ2 has low affinity for this peptide. The PDZ2-RIL peptide complex was in fast exchange; however, the data show (Figure 3(c)) specific interactions with known binding site residues in PDZ2. The dissociation constant for the PDZ2-RIL interaction was determined to be ~1.3 mM, again a value which should be viewed as an upper limit value due to the limited solubility of this peptide.

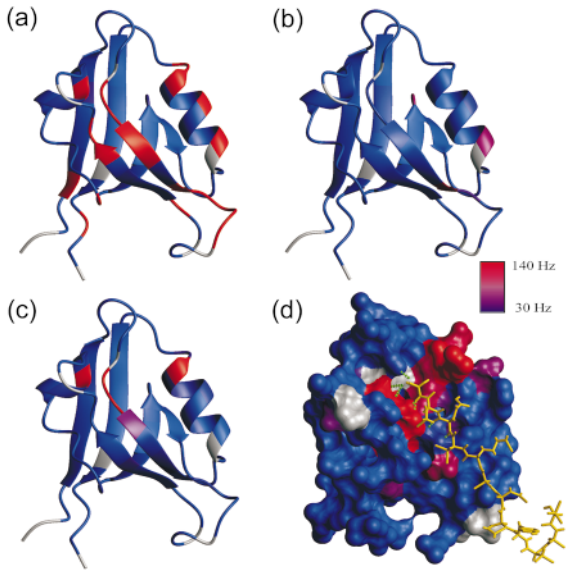

Figure 3. PDZ2 color-coded according to changes in backbone hydrogen and nitrogen chemical shift upon titration of (a) human Fas receptor, (b) mouse Fas receptor, and (c) RIL C-terminal peptides. (d) Surface representation of (c) with RIL peptide (gold) modelled into the binding pocket. According to the given scale, the blue-to-red gradient of the surface coloring represents smaller to larger changes in chemical shift. Grey coloring indicates that no data was available. Broken green lines indicate putative hydrogen bonds based on typical distance and angles constraints.

Dynamics

We performed ^{15}N relaxation measurements to probe the dynamical behavior of the PDZ2 domain. We recorded the $\{^1H\}^{15}$N-NOE, ^{15}N-T_1 and ^{15}N-$T_{1\rho}$ experiments and calculated the overall tumbling rate (τ_c), internal correlation time (τ_e) and order parameters (S^2) using a reside-by-residue fitting the relaxation rates using an isotropic diffusion model[26,27] (see Figure 4). The relaxation data were fitted and analyzed using Modelfree 4.01.[28] Of the 80 residues, 50 were fit using model 1, 13 with model 2 and seven with model 4, as displayed in Figure 4. One residue, residue 101, was not fit well by any model, and was fit with model 2. An initial estimate of the global τ_c value was optimized to 6.70 ns, a value that is typical of a compactly folded protein of this size. Regions associated with loops and turns show increased mobility, as indicated by R_{ex} and τ_e contributions. Notably, residues in the L1 loop are affected by both R_{ex} and τ_e contributions. These residues also display lower $\{^1H\}^{15}$N-NOE values which are indicative of flexibility in the picosecond timescale.

Most secondary structure elements display S^2 values above the 0.89 average. The S^2 values of β1 are lower than the average, indicating greater flexi-

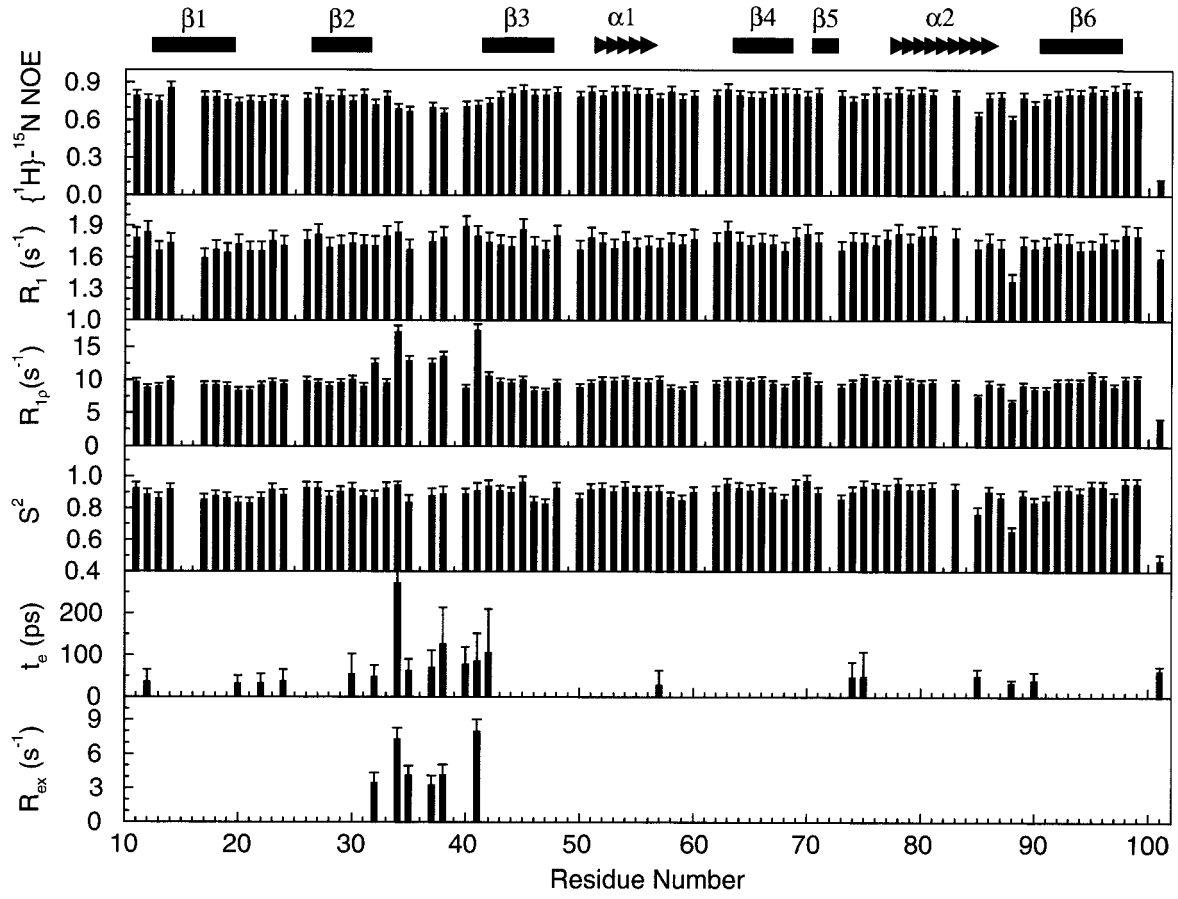

Figure 4. ^{15}N relaxation data and results of Lipari-Szabo analysis for PDZ2 as a function of residue number: $\{^1H\}^{15}$N-NOE, R_1, $R_{1\rho}$ and S^2, τ_e and R_{ex}. The secondary structure of PDZ2 is indicated at the top.

bility, perhaps explained by its location on the edge of the β-sheet. The β1-to-β2, β3-to-α1 and the α2-to-β6 turns also display S^2 values that are lower than the average. Notably, residues Leu85 and Thr88 display increased mobility with respect to neighboring residues, demonstrated by lower S^2 values and increased τ_e values. These residues also display isolated, well defined peaks in the ^{15}N HSQC and other spectra, ruling out the possibility of interference due to overlap (data not shown). These residues are located near the C-terminal cap of α2. The side-chain of Leu85 and the methyl group of Thr88 point inward while the side-chain oxygen of Thr88 faces outward.

Discussion

The PDZ2 ensemble of 35 structures is well defined with very good local geometry. We superposed PDZ2 with three X-ray structures representing the three interaction classes. This superposition shows that the PDZ fold is highly conserved among all classes despite sometimes a considerable sequence dissimilarity. To assist in quality assessment, we also superposed PDZ2 its human orthologue, PTP-Bas. Of the superposed PDZ domains, PTP-Bas was both the most sequentially similar and the most structurally dissimilar to PDZ2. A structural comparison of the PDZ2-PTP-Bas ensembles reveals several regions with significant differences in their respective ψ/ϕ dihedral angles. For instance, all β-turns in PDZ2 fall into either type I′ or II classes, whilst in the structure of the human orthologue, several of the turns are not possible to classify.[29] On all counts, comparisons of the two ensembles show that the PDZ2 compares better with data derived from current reliable X-ray structures than does the PTP-Bas, as reported by WHAT-CHECK.[25] General evaluations, such as Ramachandran quality, give much more negative values for PTP-Bas ensemble, and of particular concern are the high quantities of negative quality indicators this ensemble displays, such as interatomic clashes and unpaired hydrogen bond donors/acceptors. Comparing (RMS) *Z*-scores clearly show that PDZ2 is statistically a more reasonable ensemble than that of PTP-Bas. Including electrostatic terms in the PDZ2 refinement procedure contributed to a well-defined PDZ2 ensemble. These terms are typically implemented

incorrectly in structure refinement protocols, and frequently resulting in poor local geometry for NMR structures. The modified procedure used here will be reported elsewhere.[30]

The extended L1 loop of PDZ2 folds back onto the backbone, a unique structural feature that PTP-Bas shares. Lower $\{^1H\}^{15}N$-NOE values and chemical exchange contributions to $T_{1\rho}$ clearly confirm L1 has increased flexibility with glycine hinges contributing to this flexibility, refuting data previously reported for PTP-Bas.[31] It is conceivable that this flexibility could assist in binding target selectivity, since this effect has already been demonstrated for alternative L1-splicing.[5]

The dynamic properties of PDZ2 show a normal pattern; secondary structures are more rigid and loop structures are more flexible. Of interest are the dynamic properties of Leu85 and Thr88. Both possess low S^2 values when compared to surrounding residues, and τ_e contributions on the order of 30-50 ps. Leu85 is located near the C-terminal end of α2, while Thr88 is located in a turn-like region just as the strand exits α2. Leu85 participates in an α-helical hydrogen bonding pattern; the amide of Leu85 participates in hydrogen bonding with the carbonyl of Ala81. The side-chain oxygen atom of Thr88 is hydrogen-bonded to the amide of Leu85, suggesting that the flexibility of these two residues is linked. Comparisons with other PDZ complexes show that Leu85, in conjunction with Leu25 and Ile27, form a hydrophobic pocket that interacts with the terminal hydrophobic residue of bound C termini. Leu85 and Thr88 are found in a region that is structurally conserved (Figure 2(c)), allowing for the possibility that the mobility of these two residues has a functional significance.

Murine PDZ2 specifically binds to peptides derived from C termini of both human Fas receptor and the RIL protein with respective dissociation constants of 0.2-0.5 and ~1.3 mM. The complex with the human Fas receptor was in the intermediate exchange and with RIL in the fast exchange regime. Because the amounts of human Fas and RIL peptides available for interaction with PDZ2 were limited by solubility, these dissociation constants should be viewed as upper limits, the actual binding affinities are most likely greater than observed. Of the three peptides, the greatest affinity for the human Fas receptor peptide was expected because it contains a known PDZ-binding class 1 sequence, and has previously been shown to bind the human orthologue of PDZ2.[7,8] We modelled the RIL peptide into the PDZ2 binding pocket to clarify why its modified class 1 sequence (-E-L-V) is able to bind to PDZ2 with specific interactions in the binding pocket. The chemical shift changes correlate strongly with modelled peptide interactions. Eight putative hydrogen bonds with PDZ2 and the RIL peptide (based on angle and distance constraints) involve the carboxyl and amide groups of the modelled peptide residues 0 and −2 (Figure 3(d)). All of these hydrogen bonds agree with previously reported hydrogen bonding interactions.[32] Based on homology, a 180° plane flip of His78 upon peptide binding would permit interaction between the its N1 nitrogen and the side-chain of the −2 residue. The model, being based on the free protein, does not display this interaction. The model also does not readily suggest the formation of hydrogen bonds to other side-chain atoms; the lack of these interactions could give reason to the comparative weakness of the observed RIL interaction. The side-chain of the −2 glutamic acid points out of the binding pocket toward α2, illustrating why both serine and the bulkier glutamic acid side-chains are tolerated in this position. These results confirm previous reports of PDZ2-RIL interaction and support a C-terminal contribution to this interaction.[2] Because the RIL C terminus occupies the canonical binding site of PDZ2, we postulate that PDZ2 contains a second binding site that interacts with the LIM domain. The RIL-LIM domain contains a long, flexible tail of more than 20 residues that would provide enough conformational freedom to allow the LIM domain to reach such an alternate binding site. The mouse Fas receptor does not contain a canonical PDZ binding sequence and interacts only weakly and non-specifically with murine PDZ2. Contrary to the human and mouse Fas receptors, the sequence for the human and mouse RIL C termini are identical, suggesting a functional conservation. In addition, the absence of interaction between murine PDZ2 and its Fas receptor suggests that the Fas receptor is an unlikely *in vivo* target for PDZ2, supporting previous results.[9]

In conclusion, we reported the structure, dynamics and binding characteristics of the PDZ2 domain of PTP-BL. These data represent an essential step in elucidating the interactions mediated by the PDZ domains of PTP-BL, in particular those with LIM domain-containing proteins.

Materials and Methods

Sample preparation

The protein construct contained eight residues of a His tag (Met + 6 His + Met) and 94 residues encompassing the PDZ2 domain (residues 1351 to 1444, accession number NP_035334) inserted into a modified pET28a plasmid vector.[33] Protein expression was induced at 37 °C under kanamycin selection in *Escherichia coli* BL21(DE3) cells by addition of IPTG for four hours. The cell pellet was resuspended in a Hepes buffer (pH 7) in the presence of protease inhibitors, sonificated, and then centrifuged twice at 10000 rpm for 30 minutes to remove cell debris. The supernatant was passed through a Ni^{2+}-NTA agarose column (Qiagen) and bound protein was first washed with 20 mM imidazole and eluted with 500 mM imidazole

in Hepes buffer (pH 7.9). Selected fractions were diluted and run through a S-Sepharose fast flow cation exchange column (Amersham Pharmacia), from which the protein was eluted using a 0-1 M NaCl gradient in Hepes buffer (pH 7.0). Fractions containing the protein were then dialyzed against water, lyophilized and stored at −75 °C. Uniformly $^{15}N/^{13}C$-labelled PDZ2 samples were prepared using [^{15}N]NH_4Cl and [^{13}C]glucose as sole nitrogen and carbon sources. NMR samples contained ~1 mM dissolved protein in a buffer of 50 mM KH_2PO_4/K_2HPO_4 and 50 mM KCl (pH 6.3), $H_2O/^2H_2O$ (95%/5%), using Pefabloc and trace NaN_3 as preservative.

Peptide interactions

The peptides, ordered from Ansynth Service BV (Roosendaal), contained an N-terminal biotin group and a C-terminal carboxyl group. The peptide sequences corresponded to the final 12 C-terminal residues of three proteins, NSNFRNEIQSLV (human Fas receptor, accession number P25445), DTGNENEGQCLE (mouse Fas receptor, accession number NP_032013) and VAVYPNSKVELV (RIL accession numbers: mouse NP_062290 and human P50479). The peptides were titrated up to 3.5 mM into individual 1 mM ^{15}N-labelled protein samples. The differences in backbone HN and N chemical shifts were monitored *via* ^{15}N-HSQC spectra, recorded on the equilibrated samples at 600 MHz and 25 °C. The (initial − final) HN and N frequencies (Hz) and relative concentrations were fit using a least-squares procedure to determine dissociation constants for the peptides. For the human Fas receptor peptide, the change in peak intensity *versus* the relative concentration was used due to the intermediate exchange phenomena.

NMR spectroscopy

NMR experiments were collected at 25 °C on a double-labelled $^{13}C/^{15}N$ sample with the exception of the ^{15}N NOESY-HSQC, which was recorded on a single-labelled ^{15}N sample. The NMR experiments were carried out on Varian 500, Varian 600, Bruker 600 and Varian 750 spectrometers. The data were processed and analyzed using the NMRPipe suite[34] and XEASY.[35] The complete resonance assignment was completed using 3D HNCA, HNCO, C(CO)NH, HNCACB, HNHA, HNHB, CBCA(CO)NH, HBHA(CBCACO)NH, H(C)CH-TOCSY and (H)CCH-TOCSY experiments. The NOE assignments were completed on an aliphatic 3D ^{13}C-NOESY-HSQC and an aromatic 3D ^{13}C-NOESY-TROSY recorded on a Varian 750, and also a 3D ^{15}N-NOESY-HSQC recorded on a Bruker 600, all with mixing times of 100 ms. ^3J-coupling values were derived from 3D HNHA, HN(CO)-CO, HNCACO[N] and LRCC experiments (obtaining the $^3J(H^NH^\alpha)$, $^3J(C^{i-1}C^i)$, $^3J(H^{\alpha i}N^{i+1})$ and ^3J(CC) coupling constants). The T_1, $T_{1\rho}$ and {^{1}H}^{15}N-NOE experiments were recorded at 25 °C on a Varian 600 MHz spectrometer. The relaxation delays for duplicate T_1 experiments were $T = 0.0160$, 0.3840, 0.5120, 0.6400, 1.0240 seconds and $T = 0.0160$, 0.2560, 0.5120, 0.7680, 1.0240 seconds. The relaxation delays for the $T_{1\rho}$ experiment were $T = 0.0160$, 0.0320, 0.0480, 0.0800, 0.0960, 0.1120, 0.1280 second.

Structure refinement

The NOE peak volumes were converted into distance ranges by normalization against peak volumes that were calibrated to known distances, and then overestimated twofold. Distance restraint ranges defined with lower limits of 0 Å and upper limits of 2.8, 3.5, 5.0 or 7.0 Å. The 154 angle restraints were obtained from ^3J-couplings. The 59 hydrogen bond restraints were derived from CSI determined secondary structures and confirmed by characteristic NOE patterns. Hydrogen bonds for the HN-O and the N-O distances were restrained from 1.2-2.2 Å and 2.2-3.2 Å, respectively. An initial set of 200 NMR structures was calculated using a Cartesian-space simulated annealing protocol in X-PLOR version 3.851.[36] To improve local geometry and electrostatics, 70 lowest energy structures were then refined in water using a restrained molecular dynamics protocol under a CHARMM22 force field.[30] This resulted in a set of 43 structures with no distance restraint violations >0.5 Å and no dihedral angle violations >5°. Of these, the 35 lowest energy structures were selected to form the final ensemble. Structures were analyzed using the programs PROCHECK-NMR[23] and WHAT-IF.[24] The modelling of the RIL C-terminal peptide was accomplished using the syntrophin/nNOS interaction (PDB entry 1QAV) as a template in WHAT-IF.[24] The PDZ domains of PDZ2 and syntrophin were first superposed and then the bound interaction partner was mutated to RIL sequence. Finally, minor debumping was performed to remove steric clashes.

Data Bank accession numbers

The coordinates of the structures were deposited in the RCSB Protein Data Bank under PDB accession number 1GM1. The chemical shifts and ^{15}N relaxation data are deposited in the BioMagResBank under BMRB accession number 5131.

Acknowledgments

The modified pET28a expression vector was kindly provided by Drs N. Hanlon and D. Barford, of Oxford, UK. We thank the SON NMR Large Scale Facility (Utrecht) for the use of the Varian 750 MHz spectrometer. We also thank Professor Cees Hilbers for his interest in this project. This research was supported by NSERC (Canada) and NWO (Netherlands).

References

1. Hendriks, W., Schepens, J., Bachner, D., Rijss, J., Zeeuwen, P., Zechner, U. *et al.* (1995). Molecular cloning of a mouse epithelial protein-tyrosine phosphatase with similarities to submembranous proteins. *J. Cell. Biochem.* **59**, 418-430.
2. Cuppen, E., Gerrits, H., Pepers, B., Wieringa, B. & Hendriks, W. (1998). PDZ motifs in PTP-BL and RIL bind to internal protein segments in the LIM domain protein RIL. *Mol. Biol. Cell,* **9**, 671-683.
3. Cuppen, E., van Ham, M., Wansink, D. G., de Leeuw, A., Wieringa, B. & Hendriks, W. (2000). The zyxin-related protein TRIP6 interacts with PDZ motifs in the adaptor protein RIL and the protein

tyrosine phosphatase PTP-BL. *Eur. J. Cell. Biol.* **79**, 283-293.
4. Cuppen, E., van Ham, M., Pepers, B., Wieringa, B. & Hendriks, W. (1999). Identification and molecular characterization of BP75, a novel bromodomain-containing protein. *FEBS Letters,* **459**, 291-298.
5. Erdmann, K. S., Kuhlmann, J., Lessmann, V., Herrmann, L., Eulenburg, V., Muller, O. & Heumann, R. (2000). The Adenomatous Polyposis Coli-protein (APC) interacts with the protein tyrosine phosphatase PTP-BL *via* an alternatively spliced PDZ domain. *Oncogene,* **19**, 3894-3901.
6. Gross, C., Heumann, R. & Erdmann, K. S. (2001). The protein kinase C-related kinase PRK2 interacts with the protein tyrosine phosphatase PTP-BL *via* a novel PDZ domain binding motif. *FEBS Letters,* **496**, 101-104.
7. Sato, T., Irie, S., Kitada, S. & Reed, J. C. (1995). FAP-1: a protein tyrosine phosphatase that associates with Fas. *Science,* **268**, 411-415.
8. Saras, J., Engstrom, U., Gonez, L. J. & Heldin, C. H. (1997). Characterization of the interactions between PDZ domains of the protein-tyrosine phosphatase PTPL1 and the carboxyl-terminal tail of Fas. *J. Biol. Chem.* **272**, 20979-20981.
9. Cuppen, E., Nagata, S., Wieringa, B. & Hendriks, W. (1997). No evidence for involvement of mouse protein-tyrosine phosphatase-BAS-like Fas-associated phosphatase-1 in Fas-mediated apoptosis. *J. Biol. Chem.* **272**, 30215-30220.
10. Maekawa, K., Imagawa, N., Naito, A., Harada, S., Yoshie, O. & Takagi, S. (1999). Association of protein-tyrosine phosphatase PTP-BAS with the transcription-factor-inhibitory protein IkappaBalpha through interaction between the PDZ1 domain and ankyrin repeats. *Biochem. J.* **337**, 179-184.
11. Irie, S., Hachiya, T., Rabizadeh, S., Maruyama, W., Mukai, J., Li, Y. *et al*. (1999). Functional interaction of Fas-associated phosphatase-1 (FAP-1) with p75(NTR) and their effect on NF-kappaB activation. *FEBS Letters,* **460**, 191-198.
12. Saras, J., Franzen, P., Aspenstrom, P., Hellman, U., Gonez, L. J. & Heldin, C. H. (1997). A novel GTPase-activating protein for Rho interacts with a PDZ domain of the protein-tyrosine phosphatase PTPL1. *J. Biol. Chem.* **272**, 24333-24338.
13. Lin, D., Gish, G. D., Songyang, Z. & Pawson, T. (1999). The carboxyl terminus of B class ephrins constitutes a PDZ domain binding motif. *J. Biol. Chem.* **274**, 3726-3733.
14. Songyang, Z., Fanning, A. S., Fu, C., Xu, J., Marfatia, S. M., Chishti, A. H. *et al*. (1997). Recognition of unique carboxyl-terminal motifs by distinct PDZ domains. *Science,* **275**, 73-77.
15. Brenman, J. E., Chao, D. S., Gee, S. H., McGee, A. W., Craven, S. E., Santillano, D. R. *et al*. (1996). Interaction of nitric oxide synthase with the postsynaptic density protein PSD-95 and alpha1-syntrophin mediated by PDZ domains. *Cell,* **84**, 757-767.
16. Karthikeyan, S., Leung, T. & Ladias, J. A. (2001). Structural basis of the Na^+/H^+ exchanger regulatory factor PDZ1 interaction with the carboxyl-terminal region of the cystic fibrosis transmembrane conductance regulator. *J. Biol. Chem.* **276**, 19683-19686.
17. Daniels, D. L., Cohen, A. R., Anderson, J. M. & Brunger, A. T. (1998). Crystal structure of the hCASK PDZ domain reveals the structural basis of class II PDZ domain target recognition. *Nature Struct. Biol.* **5**, 317-325.
18. van Huizen, R., Miller, K., Chen, D. M., Li, Y., Lai, Z. C., Raab, R. W. *et al*. (1998). Two distantly positioned PDZ domains mediate multivalent INAD-phospholipase C interactions essential for G protein-coupled signaling. *EMBO J.* **17**, 2285-2297.
19. Hillier, B. J., Christopherson, K. S., Prehoda, K. E., Bredt, D. S. & Lim, W. A. (1999). Unexpected modes of PDZ domain scaffolding revealed by structure of nNOS-syntrophin complex. *Science,* **284**, 812-815.
20. Schepens, J., Cuppen, E., Wieringa, B. & Hendriks, W. (1997). The neuronal nitric oxide synthase PDZ motif binds to -G(D,E)XV* carboxyterminal sequences. *FEBS Letters,* **409**, 53-56.
21. Geijsen, N., Uings, I. J., Pals, C., Armstrong, J., McKinnon, M., Raaijmakers, J. A. *et al*. (2001). Cytokine-specific transcriptional regulation through an IL-5Ralpha interacting protein. *Science,* **293**, 1136-1138.
22. Christopherson, K. S., Hillier, B. J., Lim, W. A. & Bredt, D. S. (1999). PSD-95 assembles a ternary complex with the N-methyl-D-aspartic acid receptor and a bivalent neuronal NO synthase PDZ domain. *J. Biol. Chem.* **274**, 27467-27473.
23. Laskowski, R. A., Rullmannn, J. A., MacArthur, M. W., Kaptein, R. & Thornton, J. M. (1996). AQUA and PROCHECK-NMR: programs for checking the quality of protein structures solved by NMR. *J. Biomol. NMR,* **8**, 477-486.
24. Vriend, G. (1990). WHAT-IF: a molecular modeling and drug design program. *J. Mol. Graph.* **8**, 52-56, 29.
25. Hooft, R. W., Vriend, G., Sander, C. & Abola, E. E. (1996). Errors in protein structures. *Nature,* **381**, 272-272.
26. Lipari, G. & Szabo, A. (1982). Model-free approach to the interpretation of nuclear magnetic resonance in macromolecules: 1. Theory and range of validity. *J. Am. Chem. Soc.* **104**, 4546-4559.
27. Lipari, G. & Szabo, A. (1982). Model-free approach to the interpretation of nuclear magnetic resonance in macromolecules: 2. Analysis of experimental results. *J. Am. Chem. Soc.* **104**, 4559-4570.
28. Mandel, A. M., Akke, M. & Palmer, A. G. (1995). Backbone dynamics of *Escherichia coli* ribonuclease HI: correlations with structure and function in an active enzyme. *J. Mol. Biol.* **246**, 144-163.
29. Hutchinson, E. G. & Thornton, J. M. (1994). A revised set of potentials for beta-turn formation in proteins. *Protein Sci.* **3**, 2207-2216.
30. Spronk, C. A., Linge, J. P., Hilbers, C. W. & Vuister, G. W. (2002). Improving the quality of protein structures determined by NMR spectroscopy. *J. Biomol. NMR,* in the press.
31. Kozlov, G., Gehring, K. & Ekiel, I. (2000). Solution structure of the PDZ2 domain from human phosphatase hPTP1E and its interactions with C-terminal peptides from the Fas receptor. *Biochemistry,* **39**, 2572-2580.
32. Doyle, D. A., Lee, A., Lewis, J., Kim, E., Sheng, M. & MacKinnon, R. (1996). Crystal structures of a complexed and peptide-free membrane protein-binding domain: molecular basis of peptide recognition by PDZ. *Cell,* **85**, 1067-1076.
33. Hoffmann, K. M., Tonks, N. K. & Barford, D. (1997). The crystal structure of domain 1 of receptor pro-

tein-tyrosine phosphatase mu. *J. Biol. Chem.* **272**, 27505-27508.
34. Delaglio, F., Grzesiek, S., Vuister, G. W., Zhu, G., Pfeifer, J. & Bax, A. (1995). NMRPipe: a multidimensional spectral processing system based on UNIX pipes. *J. Biomol. NMR*, **6**, 277-293.
35. Bartels, C. H., Xia, T.-H., Billeter, M., Güntert, P. & Wüthrich, K. (1995). The program XEASY for computer-supported NMR spectral analysis of biological macromolecules. *J. Biomol. NMR,* **6**, 1-10.
36. Brunger, A. T. (1996). *X-PLOR Version 3.851. A System for X-ray Crystalography and NMR*, Yale University Press, New Haven, CT.
37. Koradi, R., Billeter, M. & Wuthrich, K. (1996). MOLMOL: a program for display and analysis of macromolecular structures. *J. Mol. Graph.* **14**, 51-32.

Edited by M. F. Summers

(Received 27 September 2001; received in revised form 7 January 2002; accepted 7 January 2002)